Development of Fe/TiO$_2$ Photocatalyst via Precipitation Method for Hydrogen Production from Water

By

Aimi Zeti Binti Zahari

Dissertation submitted in partial fulfillment of

the requirements for the

Bachelor of Engineering (Hons)

(Chemical Engineering)

JULY 2010

Universiti Teknologi PETRONAS

Bandar Seri Iskandar

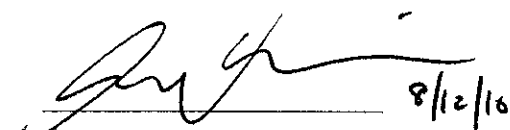31750 Tronoh

Perak Darul Ridzuan

CERTIFICATION OF APPROVAL

Development of Fe/TiO₂ Photocatalyst via Precipitation Method for Hydrogen Production from Water

by

Aimi Zeti Binti Zahari

A project dissertation submitted to the

Chemical Engineering Programme

Universiti Teknologi PETRONAS

in partial fulfilment of the requirement for the

BACHELOR OF ENGINEERING (Hons)

(CHEMICAL ENGINEERING)

Approved by,

_____

(Dr Chong Fai Kait)

Assoc. Prof. Dr. Chong Fai Kait
Fundamental and App[...] [...] Department
Universiti Tekno[...] [...]
Bandar Sari Iskan[...] [...] [...]
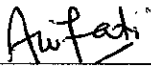Perak Darul Rid[...], MALAYSIA

UNIVERSITI TEKNOLOGI PETRONAS

TRONOH, PERAK

July 2010

CERTIFICATION OF ORIGINALITY

This is to certify that I am responsible for the work submitted in this project, that the original work is my own except as specified in the references and acknowledgements, and that the original work contained herein have not been undertaken or done by unspecified sources or persons.

AIMI ZETI BINTI ZAHARI

ABSTRACT

Hydrogen has been developed as the most promising energy sources to replace fossil fuels. The most promising renewable technologies for hydrogen production is photochemical and photocatalytic water splitting using solar energy. Pure titania (TiO_2) only absorb near-UV light which has wavelength 388 nm or less. It is not economically feasible to use UV light for hydrogen production. Doped TiO_2 with metals will enhanced the photocatalytic activity of TiO_2. The main objective of this project was to develop Fe-TiO_2 photocatalyst via precipitation method to produce hydrogen from water under visible light. This research covered preparation of iron-doped TiO_2, finding the optimum calcination temperature, characterizing the photocatalyst prepared and determining the photocatalytic activity of Fe-TiO_2 for hydrogen production from water. Fe-TiO_2 was produced using precipitation method with different iron loading which were 0.1, 0.5 and 1.0 wt% calcined at different temperature ($300^{\circ}C$, $400^{\circ}C$ and $500^{\circ}C$) for one hour. The photocatalytic study was performed at room temperature using a multiport photocatalytic reactor irradiated by 500-W halogen lamp. Characterization of the photocatalysts was done by Thermogravimetric Analyzer (TGA), Diffuse Reflectance UV-Vis (DR-UV-Vis), Field Emission Scanning Electron Microscopy (FESEM), Fourier Transform Infrared (FTIR), and X-ray Diffraction (XRD). It was found that 0.5wt% calcined at $300^{\circ}C$ evolved the highest hydrogen from water (5.75 mL). Fe/TiO_2 lowered the band gap, resulting in increasing of hydrogen production from water. The reduction of band gap as a result of doping was estimated and the effects of the parameters (Fe loading and calcination temperature) on photocatalytic activity are explained.

ACKNOWLEDGEMENT

First and foremost, highest thank to The Almighty for giving the author the strength and patience to complete this Final Year Project.

Also a heartfelt appreciation outstretch to parents, Mr. Zahari Mamat and Mrs. Asiah Daud for always being there when in need. Their guidance, love and emotional support are highly appreciated.

Uncountable appreciation extended to Dr. Chong Fai Kait for being a gratifying supervisor with kind guidance, practical criticism and valuable advice throughout the project duration of 28 weeks. Utmost gratitude also goes to Final Year Project Coordinator, Dr. Khalik and Dr. Mohanad for providing her with all the initial information required to begin the project.

Great big thanks also extended to other family members and fellow friends who had in one way or another contributed to the success of this report. Thank you again to all, your kindness and helps will always be remembered.

TABLE OF CONTENT

LIST OF FIGURES

LIST OF TABLES

CHAPTER 1

INTRODUCTION

1.1   PROJECT BACKGROUND

In recent years, fossil fuels have become the major source of energy. However, as time goes on, fossil fuels are depleting and have a bad environmental impact of burning fossil fuels. Environmental problems such as Earth's climate change, greenhouse effect and air pollution have been major issues around the world. A lot of researches have been done to find and replace the fossil fuels.

It is importance to identify alternative energy sources that can replace these fossil fuels. Renewable energy sources such as hydrogen have been seen as the future main energy source. Most importance, this renewable energy does not generate any greenhouse effect to the environment. Hydrogen can be produced from fossil fuels as well as from biomass. However, by using alternative sources such as solar energy, this technology can provide a sustainable solution to both energy and environmental issues. Alternative energy and renewable energy sources such as solar energy, biofuels (biodiesel, biomass, and methanol), wind energy, and hydrogen energy have been studied and developed over years to find the best alternative energy sources to replace fossil fuels.

Hydrogen has been developed as the most promising energy sources to replace fossil fuels. Hydrogen can be made from renewable sources, fossil fuels decarbonized or nuclear energy. Renewable sources such as water can produces hydrogen via electrolysis. Basic process of electrolysis is by placing positives and negatives

electrodes in the water, then the water will disassociated into hydrogen and oxygen. Based on the recent studies, the most promising renewable technologies for hydrogen production is photochemical and photocatalytic water splitting using solar energy.

Catalyst is the chemical that change the rate of a chemical reaction. Photocatalyst is the catalyst that accelerates photoreaction. Lots of photocatalyst have been studied to accelerate photocatalytic water splitting. Titanium dioxide or Titania (TiO_2) has been proven to be the most suitable and good photocatalyst for water splitting (Yoong *et al.*, 2009). TiO_2 has several unique characteristic such as biological and chemical inertness, cost-effectiveness, environmental friendly and long-term stability against photo-corrosion and chemical corrosion (Liu *et al.*, 2006). However, pure TiO_2 mostly only absorbs the ultraviolet region of sunlight making it not photoactive under the illumination of visible light (wavelength from 400 to 800 nm) (Viswanathan *et al.*, 2002).

Studies and research have been done throughout the times to overcome this problem. Lots of studies focused on metal doping to the pure TiO_2. Metal such as Fe, Cu, and Cr are found to be most promising transition metal to be doped with TiO_2. Several techniques have been implemented to prepare metal-doped TiO_2 such as wet impregnation, hydrothermal, ultrasonic, solovothermal and so-gel (Liu *et al.*, 2006). However, precipitation method is the least popular method used to prepare Fe-doped with TiO_2. The main objective of this project is to develop Fe-TiO_2 photocatalyst via precipitation method to produce hydrogen from water under visible light.

This research covers preparation of iron-doped TiO_2, finding the optimum calcination temperature, characterizing the photocatalyst prepared and determining the photocatalytic activity of Fe-TiO_2 for hydrogen production from water. In the second chapter, literature review about the past studies in this area has been done for more

2

understanding. Research about pure TiO₂ and reasons for choosing iron as the metal dopant is explained thoroughly in this chapter. Research about other metals such as copper and chromium is also explained.

Third chapter covers the methodology of the experimental research and the preparation of photocatalyst. In this study, the method used to prepare the Fe-TiO₂ photocatalyst is precipitation method using chemicals which are glycerol, iron nitrate, titania Degussa P25 and sodium hydroxide. Later on, the catalyst will be tested using TGA, DR-UV-Vis, FESEM, FTIR and XRD to determine the chemical and physical properties of the catalyst. Photocatalytic activity is performed using a multiport photocatalytic reactor.

The results obtained from the characterization test and photocatalytic activity are presented in Chapter 4. Using photocatalytic reaction data, comparison for each sample is done to determine the best calcinations temperature and optimum metal loading. A few samples then were sent for characterization test. Result for TGA, FESEM, XRD and DR-UV-Vis are being discussed thoroughly.

In the last chapter which is Chapter 5, the conclusion of the project based on the result and discussion. In this chapter, there are also recommendations for improvement of project in future.

1.2 PROBLEM STATEMENT

Pure titania only absorb near-UV light which has wavelength 388 nm or less. It is not economically feasible to use UV light for hydrogen production. Since pure titania is not photoactive under visible light, several ways has been implemented to extend its activity region to the visible light region. One of the methods is by doping titania with transition metals. Doping with metal ions may extend the photo-response of TiO_2 into the visible spectrum by reducing the band gap of TiO_2. In this research project, Iron has been chose to be the transition metal to be doped with TiO_2 as photocatalyst for hydrogen production from water. Precipitation method is used as the method to prepare the photocatalyst.

1.3 OBJECTIVES AND SCOPE OF STUDY

The objective of this research project is:

1. To develop Fe-TiO_2 photocatalyst to produce hydrogen from water under visible light

The scopes of study for this research study are:

1. To prepare Fe/TiO_2 photocatalyst using precipitation method with different Fe loading and pretreatment conditions (calcination temperature)
2. To determine optimum Fe loading in the photocatalyst and the calcination temperature that produce maximum rate of hydrogen production from water
3. To characterize the photocatalyst using FESEM, XRD, DR-UV-Vis, FTIR, and TGA
4. To determine the performance of Fe-TiO_2 for hydrogen production from water

CHAPTER 2

LITERATURE REVIEW AND THEORY

2.1   PHOTOCATALYST

Catalyst is the chemical that change the rate of a chemical reaction. Catalyst aid the attainment of chemical equilibrium by reducing the potential energy barriers in the reaction path. The speed of catalyzed reaction is described as a 'turn-over rate', which reveals how many reactant molecules are converted on an 'active site' or on a unit catalytic surface area per second at a given temperature, pressure and concentration of reactant and product (Viswanathan et al., 2002). It is believed that the higher surface area of catalyst, the higher will be the activity.

Photocatalyst is the catalyst that accelerates photoreaction. Example of photocatalyst is oxides such as TiO_2, $SrTiO_3$, Fe_2O_3 and Titanates; cadmium sulfide, nitrides, oxynitrides and oxysulfides (Gupta, 2008). Photocatalyst has widely environmental applications such as in photocatalytic water splitting, air purification, water disinfection, water purification, hazardous waste remediation, and much more (Liu et al., 2006).

2.2   TITANIUM DIOXIDE OR TITANIA

Titanium dioxide or also known as Titania (TiO_2) is a harmless chemical widely applied in various fields such as paints and toothpaste. Titania has been studied and has been considered as a good photocatalyst. Titania has characteristics such as inertness to chemical and biological, strong oxidation power, cost-effective and long-term stability

5

against photo-corrosion and chemical corrosion (Liu *et al.*, 2006). Table 2.1 lists examples of organic substances that can be degraded using TiO_2 photocatalysis.

Table 2.1: List of Photocatalytic degradation of organic substrates using TiO_2
(Viswanathan *et al.*, 2002)

Class	Examples of substances mineralized
Alkanes	Methane, isobutene, heptanes, cyclohexane
Halo alkanes	Chloromethane, Br, Cl, F subtitued ethane
Aliphatic alcohols	Methanol, ethanol, sucrose
Aliphatic carboxylic acid	Formic acid, propanic acid, oxalic acid
Alkenes	Propenes, cyclohexene
Aromatic hydrocarbons'	Benzene, naphathalene
Substituted aromatic hydrocarbons	Cholobenzene, substituted nitrobenzene
Phenols and substituted phenols	Phenol, catechol, resorcinol, chlorophenols
Aromatic carboxylic acid	Benzoic acid, phthalic acid, salicylic acid
Polymers	Polyethylene
Dyes	Methylene blue, methyl orange
Pesticides	DDT, Lindane, Parathion

There are three kinds crystal structure of Titania; rutile, anatase and brookite (Yoong *et al.*, 2009). Rutile is the high temperature type, while anatase is the low temperature type. Anatase is the most active and widely used as photocatalyst due to its stable photoactivity and prolonged lifetime (Yoong *et al.*, 2009). The anatase type with good crystallinity, small grain size and high specific surface area (Liu *et al.*, 2006) show higher photocatalytic activity compared to the other two (Lingsebigler *et al.*, 1994). Titania (anatase phase) has been recognized as a better photocatalyst in heterogeneous photocatalysis as it has a good UV absorption capacity and a good adsorption capacity for the substrates (Viswanathan *et al.*, 2002).

Several different commercially titania powders available in the market. However, Titania Degussa P25 has been generally referred to as the standard reference for other titania powder because this powder shows the highest H_2 production in photocatalytic activity. According to Kirchernova *et al.* (2005), Degussa P25 powder consisting of a mixture of anatase and rutile in proportion of 70/30% is characterized by a specific surface area (SSA) of the order of 50 m^2/g and particle size of ~30 nm. Table 2.2 summarizes the characteristics of Degussa P25 powder.

Table 2.2: Characteristic of Degussa P25 powder (Kirchernova *et al.*, 2005)

Characteristic	Degussa P25
Preparation method	Flame pyrolysis of $TiCl_4$
Composition by XRD	70% anatase / 30% rutile
Apparent powder density (g/ml)	0.05
Primary crystallite size, XRD (nm)	30
Morphology	Heterogeneous, wrinkled surface
Apparent particle size (μm)	<10
SSA_{BET} (m^2/g)	50
Weight loss on calcination (%)	<2 (1273 K)
Nitrogen adsorption isotherm	Hysteresis from 0.8 to 1 P/P_o
Pore volume (ml/g)	0.15
Pore size distribution	Little porosity, peak at 31.5 nm
Light adsorptive characteristics	Peak at about 250 nm
Phase transformation by milling	Fast to rutile only (in 12 h)
Particle size in water (μm)	0.7 – 10 (70%), 50 – 100 (10%); 5
Thermal stability	Increase in rutile content >673 K, lower photoactivity

Even though Titania can be effectively photoexcited under band gap irradiation, Titania alone becomes inactive. Titania becomes inactive under the illumination of visible light that has wavelength from 400 to 800 nm as its band edge absorption's threshold is $\leq$400 nm (Viswanathan et al., 2002). The band gap for titania is Eg = 3.0 – 3.2 eV (Rajeshwar et al., 2006). Only a small fraction (about 4-5%) of solar radiation can be harnessed by Titania. It only absorbs energy from near-UV light which has wavelength approximately from 388 nm and less (Yoong et al., 2009). Therefore, this absorption edge needs to be extended to the visible range if the photocatalyst is to be used in applications which involve direct sunlight. So far, band gap narrowing by using dopant is one of the most investigated methods to achieve this goal.

To increases the photoactive of TiO_2 and extend its light absorption moving from UV light to visible light region, various transition metal and non-metal have been doped into Titania (Zhou et al., 2006). The photocatalytic activites also depends on the method of metal loading (Viswanathan et al., 2002). Dholam et al. (2009) reported that Cr-doped TiO_2 and Fe-doped TiO_2 prepared using magnetron sputtering method were much more efficient than those prepared using sol-gel method. Several techniques have been implemented to prepare metal-doped TiO_2 such as hydrothermal treatment, wet impregnation, sol-gel (Liu et al., 2006), ultrasonic, solvothermal and complex precipitation (Yoong et al., 2009). Doping metal onto TiO_2 increases the minority (hole) carrier diffusion length therefore permitting an increases in the collection of photogenerated charge. In addition, doping can introduce or modify the surfaces states that are essential for oxidation of OH (Grimes et al., 2008).

The extent of metal loading influences the photocatalytic activitiy. The extend of loading is important in governing the net effect of metallization, with heavy metal loading leading to faster electron-hole recombination (Viswanathan et al., 2002).

8

2.3 PRINCIPLE OF PHOTOCATALYSIS

According to Grimes *et al.*, (2008), electrolysis is a process of detaching or dissociating bonded elements and compounds by passing them an electric current. Water electrolysis decomposes H_2O into hydrogen and oxygen gas. Photoelectrolysis describes electrolysis by the direct use of light – the conversion of light into electrical current and then the transformation of a chemical entity (H_2O, H_2S, etc) into useful chemical energy (H_2) using the current. Photoelectrolysis integrates solar energy collection and water electrolysis into a single photoelectrode (Grimes *et al.*, 2008).
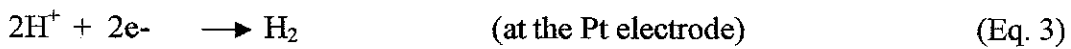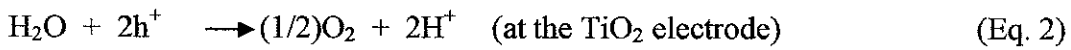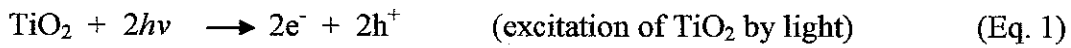
Water splitting using photocatalyst has been studied in the research fields of catalysis, electrochemistry, photochemistry, organic and inorganic chemistry, etc. for about 30 years since the Honda-Fujishima effect reported in 1968 using a TiO_2 semiconductor electrode (Kudo, 2005). Water-splitting reaction has an overall energy requirement as the water molecule is in fact very stable (Mansor, 2008), with a heat of formation of - 285.83 kJ mol^{-1} under standard conditions (Rand *et al.*, 2008). Decomposition by direct heating only starts to become significant at very high temperature, namely ~1 vol.% at 2000°C. It is difficult to separate hydrogen and oxygen at such high temperature (Rajeshwar *et al.*, 2006).

According to Fujishima *et al.* (2000), in solar photovoltaic cell, photogenerated electron-hole pairs are driven efficiently in opposite directions by an electric field existing at the boundary (junction) of n- and p-type semiconductors. The maximum conversion efficiency for solid-state devices that employ a single junction has reached ~24% and, for two junctions, ~30% (Fujishima *et al.*, 2000). According to Mansor (2008) in her research, ultraviolet energy produces photons that will be absorbed by the photocatalyst, thus activating it. Its activation is preceded by the formation of pairs of

electrical charges-holes in the valence band and electrons in the conductivity band (Rajeshwar *et al.*, 2006).

An n-type TiO_2 semiconductor electrode, was connected though an electrical load to a platinum black counter electrode, was exposed to near-UV light. The surface of TiO_2 was irradiated by the light with wavelength shorter than ~415 nm. Photocurrent was detected flowing from the platinum counter electrode to the TiO_2 electrode through external circuit (Fujishima *et al.*, 2000). This result proved that oxidation reaction (oxidation of oxygen) occurs at TiO_2 electrode and the reduction reaction of hydrogen at the Pt electrode. The following scheme shows the reaction:

$$TiO_2 + 2h\nu \longrightarrow 2e^- + 2h^+ \qquad \text{(excitation of } TiO_2 \text{ by light)} \qquad \text{(Eq. 1)}$$

$$H_2O + 2h^+ \longrightarrow (1/2)O_2 + 2H^+ \quad \text{(at the } TiO_2 \text{ electrode)} \qquad \text{(Eq. 2)}$$

$$2H^+ + 2e- \longrightarrow H_2 \qquad \text{(at the Pt electrode)} \qquad \text{(Eq. 3)}$$

The overall reaction is

$$H_2O + 2h\nu \longrightarrow (1/2)O_2 + H_2 \qquad \qquad \text{(Eq. 4)}$$

According to Viswanathan *et al.* (2002), "during a photocatalytic reaction, the irradiated surface of the semiconductor will act as a sink for the electrons (holes) depending upon the direction of band bending." The other charge carrier will move under the influence of the electric field into the bulk of the semiconductor or to the surface that receives the lowest intensity of incident radiation. Thus, the separation of the charge carriers namely the electrons and holes determines the efficiency of any photocatalytic reaction (Viswanathan *et al.*, 2002).

2.4   IRON-DOPED WITH TiO_2

To extend light absorption from UV range to visible light range (400-800nm), TiO_2 has been modified by doping the catalyst with various metals such as Fe, Cr, Sn, Pt, V (Zhu *et al.*, 2004). According to Zhu *et al.* (2004), "photocatalytic activities of the doped TiO_2 photocatalysts substantially depend on the dopant ion nature and concentration, besides the preparation methods, the thermal and reductive treatments."

Rajeshwar *et al.* (2004) concluded that there are three main consequences of metal-modification of TiO_2 which are:

a) Stimulation of visible light photoresponce in the host material
b) Suppression (or in some cases, enhancement) of electron-hole recombination as a result of new states introduced in the band-bap of TiO_2 by these dopants
c) Generation of catalytic sites on the TiO_2 surface that serve to store electrons for subsequent transfer to acceptor species in the solution.

Zhu *et al.* (2004) has conducted an experiment to compare between undoped TiO_2 with Fe-doped TiO_2. The result of the experiment showed that Fe-doped TiO_2 exhibited higher photocatalytic reactivity compared to undoped TiO_2. Fe-doped TiO_2 with concentration of 0.09% $FeCl_3$-TiO_2 and 0.09% $FeCl_2$-TiO_2 have higher specific surface areas and smaller crystal sizes. These criteria are important for efficient photocatalytic reactions. "Fe acting as both hole and electron traps can enhance photocatalytic activity of TiO_2" (Zhu *et al.*, 2004). Table 2.3 showed particle characteristics and photoactivities of the undoped and doped TiO_2 based on Zhu *et al.* (2004) research.

Table 2.3: Particle characteristics and photoactivities of the undoped and doped TiO_2 (Zhu *et al.*, 2004)

Sample	Crystal phase	Crystallite size (nm)	Surface area (m²/g)	UV-decolorized XRG(%)[a]	Vis-decolorized XRG(%)[b]
Undoped	Anatase	77.9	29.0	56.75	18.38
0.03% FeCl₂–TiO₂	Anatase	73.5	35.6	14.37	2.27
0.03% FeCl₃–TiO₂	Anatase	77.9	31.5	20.61	6.95
0.06% FeCl₂–TiO₂	Anatase	46.4	46.7	3.74	5.61
0.06% FeCl₃–TiO₂	Anatase	43.2	54.2	16.31	6.02
0.09% FeCl₂–TiO₂	Anatase	11.6	90.5	60.16	25.80
0.09% FeCl₃–TiO₂	Anatase	11.4	101.4	70.19	41.18
0.12% FeCl₂–TiO₂	Anatase	36.2	26.3	3.56	6.02
0.12% FeCl₃–TiO₂	Anatase	59.4	16.1	4.22	7.35
0.15% FeCl₂–TiO₂	Anatase	17.6	55.5	16.49	7.62
0.15% FeCl₃–TiO₂	Anatase	32.2	20.6	20.45	8.29

[a] After photodecolorization for 1 h, exclusive of equilibrium adsorption.
[b] After photodecolorization for 7 h, exclusive of equilibrium adsorption.

Based on Zhou *et al.* (2006), a small amount of Fe-doping could enhance the photocatalytic of TiO_2 powder. At an optimal atomic ratio of Fe:Ti of 0.25, the photocatalytic activity of Fe-doped TiO_2 powders prepared by ultrasonic method and calcined at 400°C exceed that of Degussa P25 by a factor of more than two times. This high activity of the photocatalyst is the results of the large BET specific surface area and small crystallite size.

Fe^{3+} serves as effective electron trap in anatase (Eq. 5). Meanwhile, Fe^{3+} can also serve as hole trap (Eq. 6), according to the following reactions (Zhu *et al.*, 2004) :

$$Fe^{3+} \; + \; e^{-} \; \longrightarrow \; Fe^{2+} \qquad \text{(Eq. 5)}$$

$$Fe^{3+} \; + \; h_{vb}^{+} \; \longrightarrow \; Fe^{4+} \qquad \text{(Eq. 6)}$$

Dholam *et al.* (2009) had made researched on Fe- and Cr doped TiO_2 prepared using two methods, which were radio-frequency magnetron sputtering and sol-gel method. They reported that metal-doped by sputtering method was much more efficient than sol-gel method. Table 2.4 showed that the shifted band gap TiO_2 after being doped with both metals. For sputtering method, the optical band gap was much lower than TiO_2 prepared using sol-gel method. Comparing Fe and Cr, Fe ions has lower band gap in

both methods. The results also showed that H_2 production rate is higher for Fe-doped than Cr-doped because Fe ions able to trap both electrons and holes, while Cr only trap one type of charges carrier. This proved that Fe is a better dopant for TiO_2 therefore increasing the photocatalytic activity.

Table 2.4: The energy values of the fundamental band gap and impurity levels obtained after doping TiO_2 films, synthesized with sputtering and sol-gel methods, with Cr and Fe at different atomic concentration. R= fitting coefficient. (Dholam *et al.*, 2009)

Sputter-deposited TiO_2 films			Sol–gel deposited TiO_2 films		
Metal concentration (at.%)	TiO_2 optical band gap (eV)	Impurity energy level (eV)	Metal concentration (at.%)	TiO_2 optical band gap (eV)	Impurity energy level (eV)
Pure TiO_2	3.21 ($R^2 = 0.999$)	2.85 ($R^2 = 0.997$)	Pure TiO_2	3.41 ($R^2 = 0.994$)	
0.8 Cr%	3.01 ($R^2 = 0.996$)	–	0.5 Cr%	3.38 ($R^2 = 0.998$)	–
1.2 Cr%	2.38 ($R^2 = 0.991$)	–	1 Cr%	3.32 ($R^2 = 0.996$)	2.51 ($R^2 = 0.999$)
3.8 Cr%	2.24 ($R^2 = 0.999$)	–	2 Cr%	3.31 ($R^2 = 0.995$)	2.39 ($R^2 = 0.999$)
5.2 Cr%	2.19 ($R^2 = 0.999$)	–	5 Cr%	3.19 ($R^2 = 0.994$)	2.21 ($R^2 = 0.998$)
0.4 Fe%	3.13 ($R^2 = 0.996$)	–	0.5 Fe%	3.45 ($R^2 = 0.998$)	–
1.1 Fe%	3.02 ($R^2 = 0.994$)	–	1 Fe%	3.44 ($R^2 = 0.999$)	–
4.9 Fe%	2.83 ($R^2 = 0.999$)	–	2 Fe%	3.43 ($R^2 = 0.999$)	–
			5 Fe%	3.22 ($R^2 = 0.998$)	–

2.5   PRECIPITATION METHOD

Precipitation method is the conversion of highly soluble metal precursor into another substance of lower solubility, which specifically precipitates onto a support. The conversion of low soluble compound, and then into the precipitate, is usually achieved by raising the pH of the solution (Viswanathan *et al.*, 2002). In principle, this method of preparation enables the interaction between the metal precursor and the support leads to the formation of highly dispersed active phase after thermal treatment.

Calcination or also known as annealing, thermolysis or pyrolysis exposes the as-prepared catalyst precursor to high temperature for final step in the formation of finished catalysts. According to Viswanathan *et al.* (2002), there are several purposes for

calcinations. The primary used of calcinations is to thermally decomposed nonoxidic precursor and remove unwanted ligands. Precursor counterions consisting of hydrogen, carbon, or nitrogen often volatilize in the furnace and are swept away, leaving an impurity-free surface. Counterions such as alkali and alkaline metals mostly remainon the surface, and, if not washed, can participate as promoters or poisons in the final catalyst. The thermal energy of calcinations also controls the crystalline phase and grain size of the surface (Viswanathan *et al.*, 2002).

CHAPTER 3

METHODOLOGY

3.1 PROCESS FLOW

This project is an experiment-based project. The entire results can only be gained by completing lab experiments. This project contains several important steps which involve problem definition/identification, research regarding the topics, literature review, processing the material, data analysis and result. The flow chart below shows the entire steps in this project.
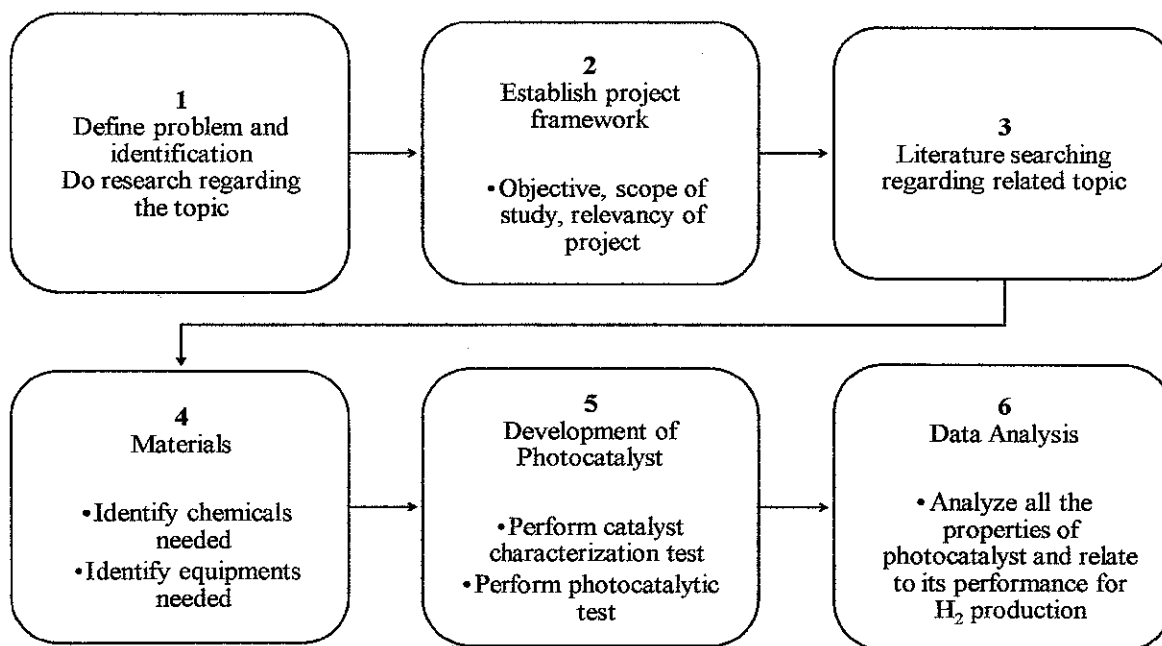

Figure 3.1: Flow Project

3.2 MATERIALS

Fe-doped TiO_2 photocatalyst samples are required for the research. Experiments to produce Fe-doped TiO_2 will be conducted using precipitation method. Iron (III) nitrate, $Fe(NO_3)_3$ are used as metal source to be doped with TiO_2. The other raw materials needed in the process are glycerol and sodium hydroxide as precipitation agent.

3.3 EXPERIMENT TOOLS AND CHEMICALS

The following are the major tools and chemicals that will be used in the laboratory experiment for the research.

Table 3.1: Tools required for experiment

Tools	Brand
Thermogravimetric analyzer(TGA)	Perkin Elmer
Diffuse reflectance UV-Vis (DR-UV-Vis) spectrophotometer	Shimadzu 3150
Field emission - Scanning electron microscopy (FESEM)	LEO
Fourier transform infrared (FTIR) spectrometer	Shimadzu
X-ray diffractometer (XRD)	BRUKER D8 AXS
Furnace	STRUART
Oven	CARBOLITE
500 W medium pressure Halogen lamp	
Multiport Photocatalytic Reactor	Custom Made

Table 3.2: Chemicals required for experiment

Chemical	Brand	Purity
Glycerol	System	95 %
Titanium Oxide (TiO_2)	Degussa P25	70% anatase, 30% rutile
Sodium Hydroxide (NaOH)	Merck	95 %
Iron (III) Nitrate ($Fe(NO_3)_3$)	Acros	> 98 %

3.4   SAMPLE PREPARATION AND EXPERIMENTS

3.4.1   Preparation of Fe-doped TiO_2 (Fe/TiO_2)

Iron-doped TiO_2 (Fe/TiO_2) can be produced using several methods such as precipitation, sol-gel, magnetron sputtering, hydrothermal hydrolysis wet impregnation method. In this research, Fe/TiO_2 is produced using precipitation method with different iron loading. The chemicals used are glycerol, titania Degussa P25, Iron (III) nitrate, and sodium hydroxide. Iron (III) is used as iron source. For the precipitation of Fe onto TiO_2, sodium carbonate, NaOH is used as the precipitating agent.

Iron (III) nitrate, $Fe(NO_3)_3.9H_2O$ is weighed then dissolved in 100 ml of distilled water. Glycerol is added to an aqueous solution of Fe (Fe:Glycerol mole ratio = 1:2) while being continuously stirred with magnetic stirrer at room temperature. Then, TiO_2 is added to the solution with continuous stirring to form a suspension. The iron-glycerol is precipitated on TiO_2 particles by adding 280 ml of sodium hydroxide, NaOH (0.25 M) dropwise into the suspension with constant stirring. The precipitate formed is further stirred intensely for 30 min. The precipitate are then filtered using a filtration unit and dried overnight at 70°C in an oven. The raw materials are calcined at 300°C, 400°C or 500°C for one hour in a muffle furnace.

Figure 3.2 showed the simplified flow of the experiment. Detailed calculation of the metal loading is provided in APPENDIX A. Calculation for the preparation of 0.25 M NaOH is provided in APPENDIX B.
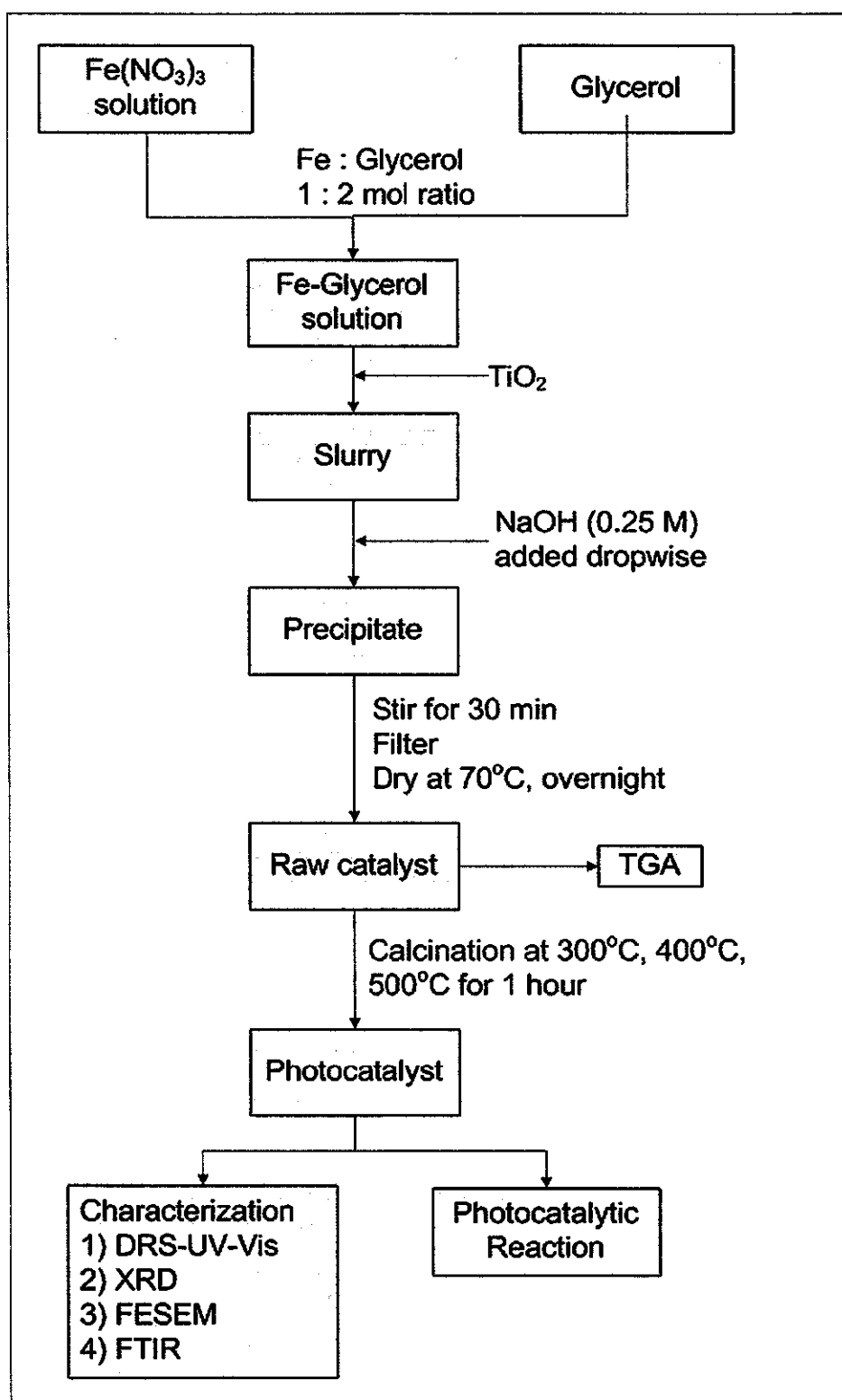
Figure 3.2: Preparation of Fe-doped TiO_2

Thermal decomposition on the raw catalyst is conducted using a thermal gravimetric analyzer (TGA) prior to calcinations to estimate the calcinations temperature. A catalyst sample is designated as mFeTa where m is the percentage of Fe loading: T refers to TiO_2 and a is the calcinations temperature ($x100^{\circ}C$). Samples with different Fe loading were prepared which at 0.1, 0.5 and 1.0 wt. %. The accuracy of measurement of weight is up to 0.01 mg and that of temperature is $\pm 1^{\circ}C$.

Fe/TiO_2 catalysts prepared are indicated in Table 3.1.

Table 3.3: Details of photocatalyst prepared

Fe loading, wt%	Calcination Temperature, $^{\circ}C$		
	300	400	500
0.1	0.1FeT3	0.1FeT4	0.1FeT5
0.5	0.5FeT3	0.5FeT4	0.5FeT5
1.0	1.0FeT3	1.0FeT4	1.0FeT5

3.4.2 Photocatalytic Activity

The photocatalytic study is performed at room temperature using a multiport photocatalytic reactor schematically shown in Figure 3.3. 0.1 g of photocatalyst sample is dispersed in a mixture of 8 ml of distilled water and placed in the multiport reactor. 500-W halogen lamp irradiated the reactor at a height of 13 cm. The reaction study was conducted for 2 hours. The amount of gas produced is recorded every 10 minutes in a vertical graduated glass tube by water displacement.
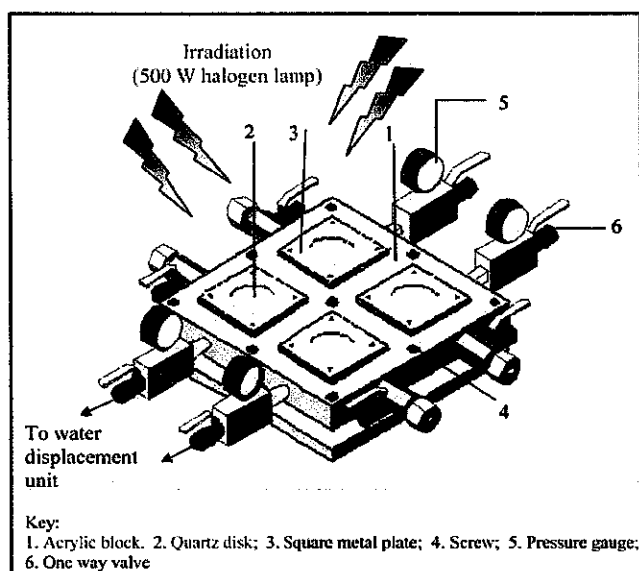
Figure 3.3: Schematic of the multiport photocatalytic reactor (Yoong *et al.*, 2009)

3.4.3 Characterization of Fe/TiO₂ Photocatalyst

Characterization of the Fe-TiO$_2$ photocatalyst is important to determine the chemical and physical properties of the photocatalyst. These properties are related to the photocatalytic performance. The characterization methods used in this project are Thermogravimetric Analyzer (TGA), Diffuse Reflectance UV-Vis (DR-UV-Vis), Field Emission Scanning Electron Microscopy (FESEM), Fourier Transform Infrared (FTIR), and X-ray Diffraction (XRD).

- **Field Emission Scanning Electron Microscopy (FESEM)**

  This test is to determine the morphology of the catalyst. It is also expected to show how well the dopant metal is dispersed onto TiO$_2$. The samples are coated with a layer of platinum-palladium before scanning at 100K magnification.

- **Thermo gravimetric Analysis (TGA)**

  This test is carried out using Perkin-Elmer TG system to determine the thermal stability of the catalyst materials prior to calcinations. TGA show the weight loss pattern of the material prepared freshly by the complex precipitation method. The TG curves are used to obtain information about the optimum calcination temperature. The rate of heating is maintained at $20^{\circ}C/min$, and the measurement is carried out from $30^{\circ}C$ to $800^{\circ}C$ with air flowing at a rate of 20 mL/min. TGA results are reported as thermograms which are plots of the percentage decomposition of the catalyst versus temperature.

- **Diffuse Reflectance UV-Vis (DR-UV-Vis)**

  Diffuse reflectance UV-Vis spectra are recorded on a Perkin-Elmer Lambda 900 instrument with an integrating sphere attachment using $BaSO_4$ powder as an internal reference. The layer of powder sample is made sufficiently thick such that all incident light is absorbed or scattered before reaching the back surface of the sample holder. Typically a thickness of 1–3 mm is required. This test is to determine the optical properties of the modified TiO_2. This is done by comparing the relative position of the catalyst's absorption edge to TiO_2 and would indicate whether the absorption edge has been successfully shifted to the visible light region.

- **Fourier Transform Infrared (FTIR)**

  FTIR spectra are useful for the determination of the functional groups (such as CH_3-, NO_3^-, -OH, C-O, etc) present in the catalysts before and after the calcinations process. The functional groups are identified by characteristic peaks in the spectrum. A sample for FTIR analysis is prepared by grinding and mixing 1 mg of the photocatalyst with 200 mg of IR-grade KBr and then the sample is pressed into a pellet using a hydraulic press. The FTIR spectrum of the sample, taken over a wavenumber range from 450 cm^{-1} – 4000 cm^{-1}, is recorded as the percentage of transmittance (%T) versus wavenumber.

21

- **X-ray Diffraction (XRD)**

  XRD test is conducted to determine the phases and crystallite sizes of the modified TiO_2 photocatalyst. X-ray diffraction patterns obtained using an X-ray diffractometer at room temperature. X-ray diffractometer with $CuK\alpha$ radiation to identify the type of Fe species and also TiO_2 phase present. Powder-XRD is conducted on the catalysts with $CuK\alpha$ radiation of 40 kV, 40 mA; 2θ angles from $10°$ to $80°$ and scan speed of $4°$/min. The XRD peaks are then compared with standards in order to determine the species present in the sample. XRD is also able to determine the Fe-phase present provided the crystallite size is in the detection limit.

CHAPTER 4

RESULT AND DISCUSION

4.1   PHOTOCATALYTIC ACTIVITY

Photocatalytic activities of Fe/TiO_2 were investigated for different metal loading and calcinations temperature. Figure 4.1 showed the hydrogen evolved for each photocatalyst. Overall observation indicates that calcinations temperature at 300°C displayed higher hydrogen production compared to 400°C and 500°C. 0.5 wt% of Fe/TiO_2 calcined at 300°C evolved the highest hydrogen form water (5.75 mL). 0.5 wt% photocatalyst both calcined at 300°C and 400°C showed high H_2 production. All photocatalyst showed higher H_2 production compared to TiO_2 which only produced 2.50 mL H_2.

Photocatalytic performance of the photocatalyst is influenced by the amount of metal loading and the calcinations temperature. The optimal value of Fe loading depend on a variety of parameters,such as the synthesis method and conditions, and also on the substrate itself (Ambrus *et al.*,2008). The increase in metal loading enhances the photocatalytic activity by inhibit the electron-hole recombination in TiO_2 (Yoong *et al.*, 2009). Fe^{3+} ions can enhance the intensity of absorption in the UV-light region and make a red shift in the band gap transition of the Fe-doped TiO_2 samples (Zhou *et al.*, 2006). This can caused more photo-generated electrons and holes to participate in the photocatalytic activity (Zhou *et al.*, 2006). However, further increase in metal loading (1.0 wt%) reduced of H_2 produced. When the dopant concentration is too high, the recombination rate will increase because the distance between trapping sites of particles decreases (Zhu *et al.*, 2004). The result showed that the optimum Fe loading is 0.5 wt%.
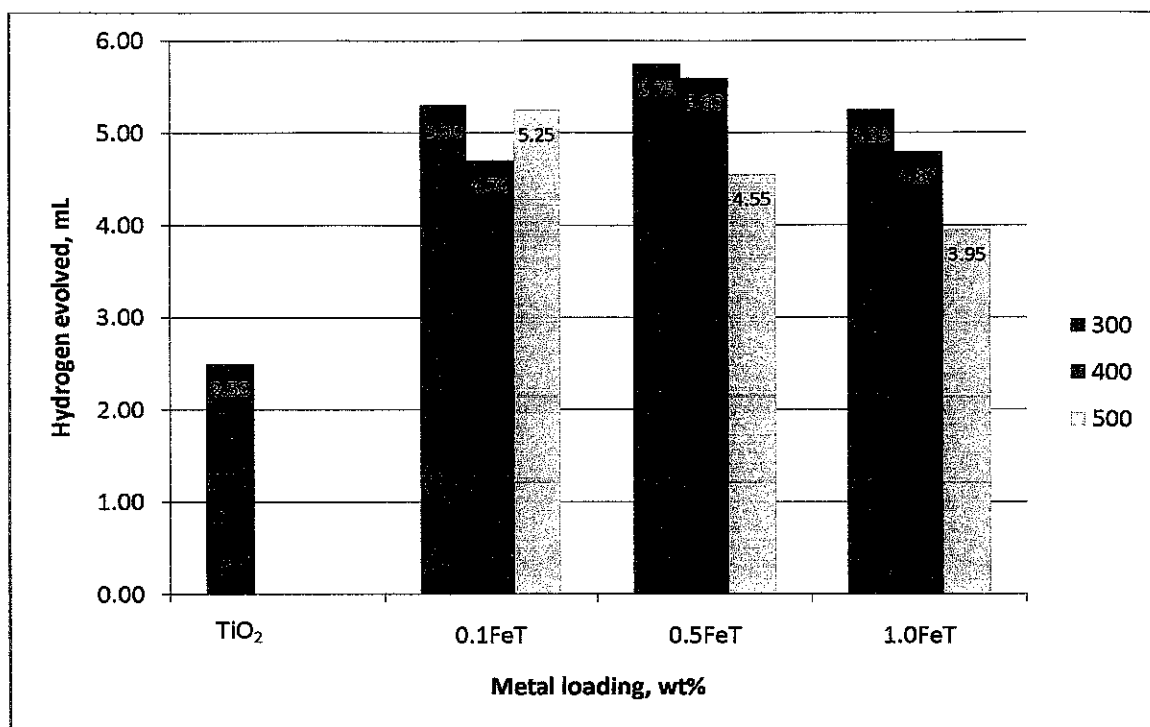
Figure 4.1: Hydrogen evolved with FeTiO₂ in distilled water

In terms of calcinations temperature, both photocatalytic activities for 0.5 wt% and 1.0 wt% samples decrease with the increase in calcination temperature from 300°C to 500°C. This may be due to the growth and agglomeration of the particles in the photocatalyst, thus reduce the contact area of the particles (Yoong *et al.*, 2009). A higher calcination temperature causes the formation of large particles and lesser contact area of Fe particles and TiO₂ (Yoong *et al.*, 2009). Before calcination, there is very low photocatalytic activity observed for pure TiO₂. The enhancement of photocatalytic activity at elevated temperature caused obvious improvement in crystallization or relative anatase crystallinity (Zhou *et al.*, 2006).

4.2 CHARACTERIZATION OF Fe/TiO$_2$

4.2.1 Thermo Gravimetric Analysis (TGA)

Thermal gravimetric analysis is performed to analyze the thermal behavior of the raw Fe-TiO$_2$ photocatalyst. The thermogram graph showed a relative weight percentage for each Fe-loading of photocatalyst prepared versus temperature. The temperature range is from 25°C to 800°C. For 0.1 wt% Fe/TiO$_2$ raw catalyst, the total weight loss was about 5.9% and for 0.5 wt% raw catalyst, the total weight loss is 6.1% and 7.9% for 1.0 wt% raw catalyst.

The larger weight losses occurred at temperature below 120°C is due to the evaporation of the physically retained or absorbed water (Zhou *et al.*, 2006). The second stage is from 120 to 820°C is due to thermal decomposition of the un-hydrolyzed ferric nitrate (Zhou *et al.*, 2006).

This thermogram curves are used to obtain information about the optimum calcinations temperature for the photocatalyst. Estimated minimum calcinations temperature of the photocatalyst is 300°C onwards since the weight loss is not too drastic after 300°C.
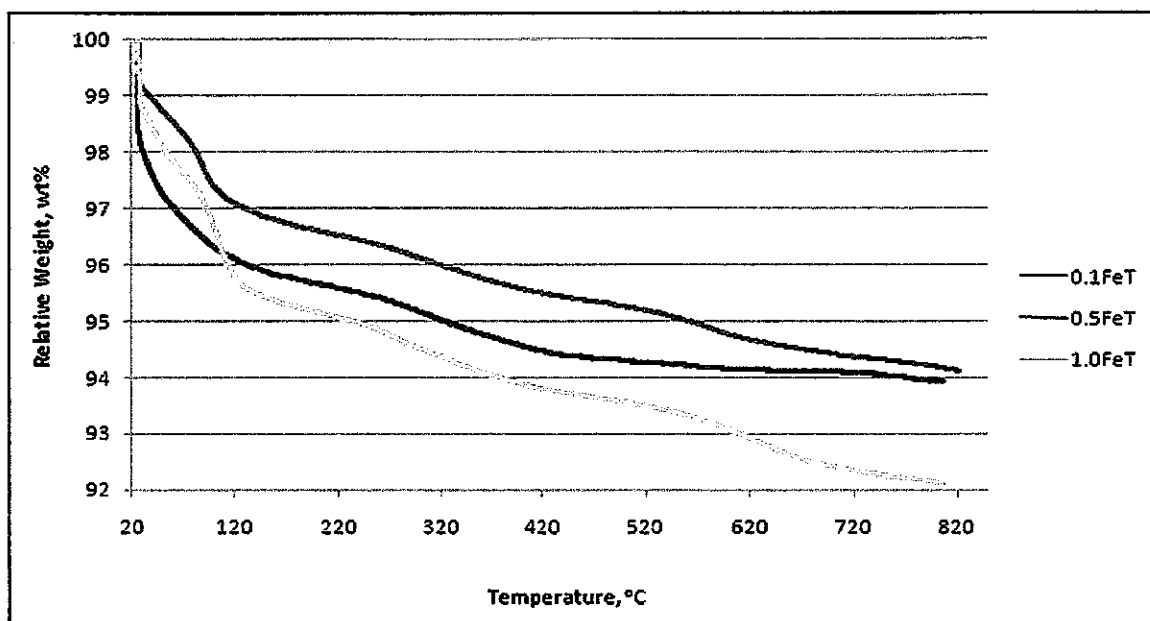
Figure 4.2: Thermal decomposition of Fe-TiO$_2$ raw catalyst for different Fe loading

4.2.2 Fourier Transform Infrared Spectroscopy (FTIR)

Figure 4.3 – 4.5 shows the FTIR transmission spectra of the Fe/TiO$_2$ photocatalyst calcined at 300°C, 400°C and 500°C. Based on observation, all the spectra have absorption peaks around 1600 cm^{-1} and 3400 cm^{-1}. Both peaks are attributed to O-H bending and stretching respectively (Yoong et al., 2009). The band observed between 400 – 900 cm^{-1} correspond to the Ti-O stretching vibrations (Yoong et al., 2009).

Absorption peak at 1280 – 1520 cm^{-1} represent the nitrate (NO$_3^-$) group. All spectra have the NO$_3^-$ peak indicating that the calcination process was not able to completely remove the NO$_3^-$ group from raw catalyst. CO$_2$ peak around 2300 cm^{-1} also been observed in some of the spectra. CO$_2$ that been detected was CO$_2$ that exist in atmosphere.
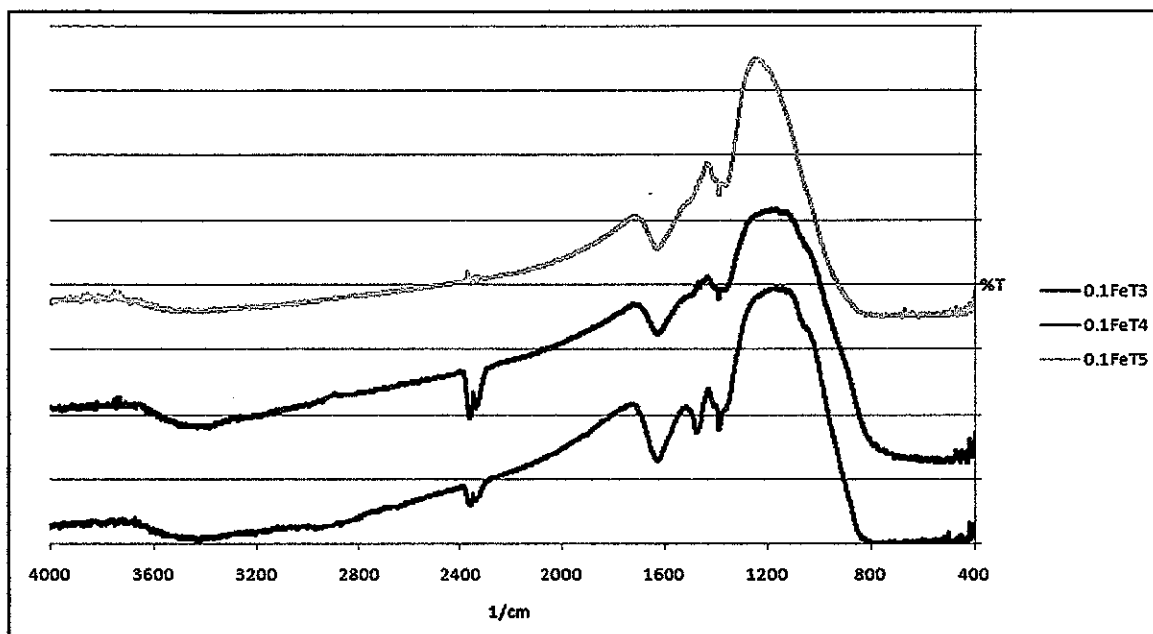
26

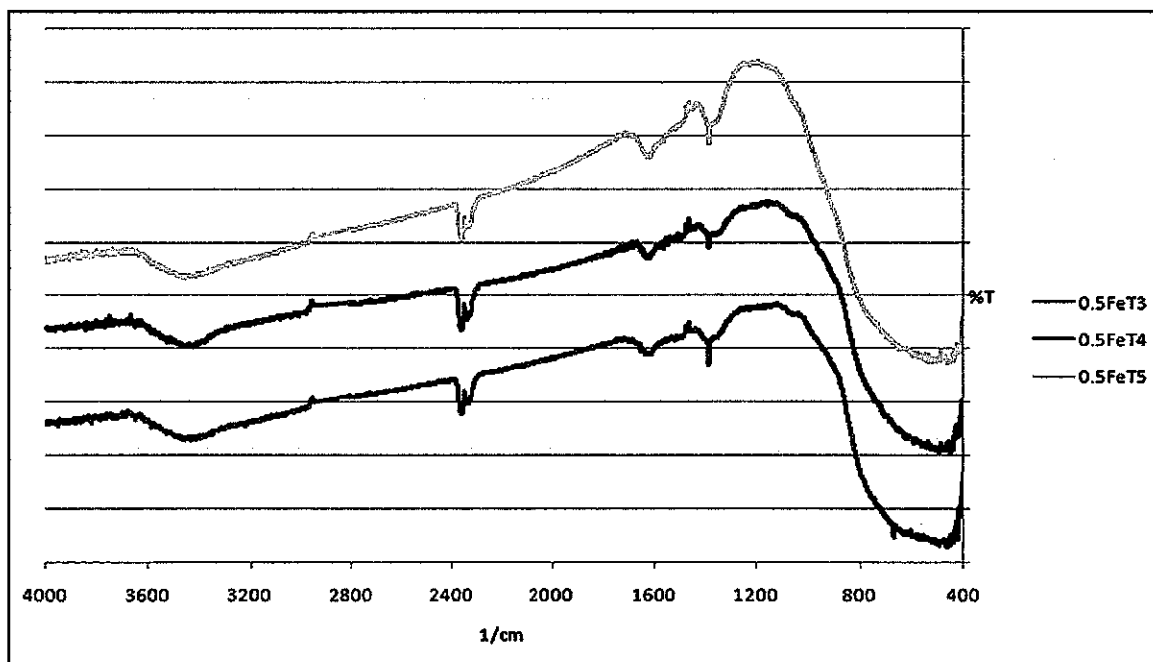Figure 4.3: FTIR transmission spectra for 0.1 wt% loading Fe/TiO_2 photocatalyst

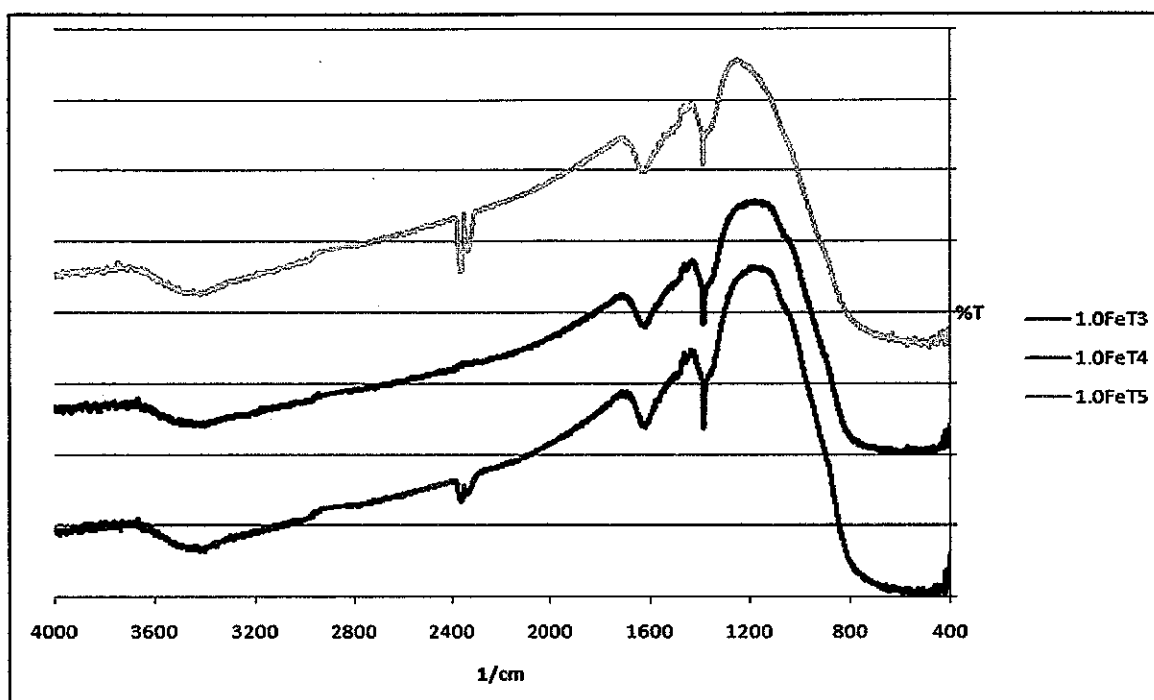Figure 4.4: FTIR transmission spectra for 0.5 wt% loading Fe/TiO_2 photocatalyst

Figure 4.5: FTIR transmission spectra for 1.0 wt% loading Fe/TiO_2 photocatalyst

4.2.3 Diffuse Reflectance UV-Vis (DR-UV-Vis)

The optical properties of the pure and iron-doped TiO_2 are studied by measuring the adsorption spectra ranging from 190 nm to 800 nm. The results are presented in Figure 4.3. The figures clearly show a shift in absorption band edge towards longer wavelength when increasing the metal concentration doped to TiO_2. The absorption threshold for pure TiO_2 was 388 nm. The absorption threshold for Fe-doped TiO_2 has been shifted towards visible region (400 nm – 800 nm). This has proven that active region of TiO_2 has been extended into the visible region when doped with iron.
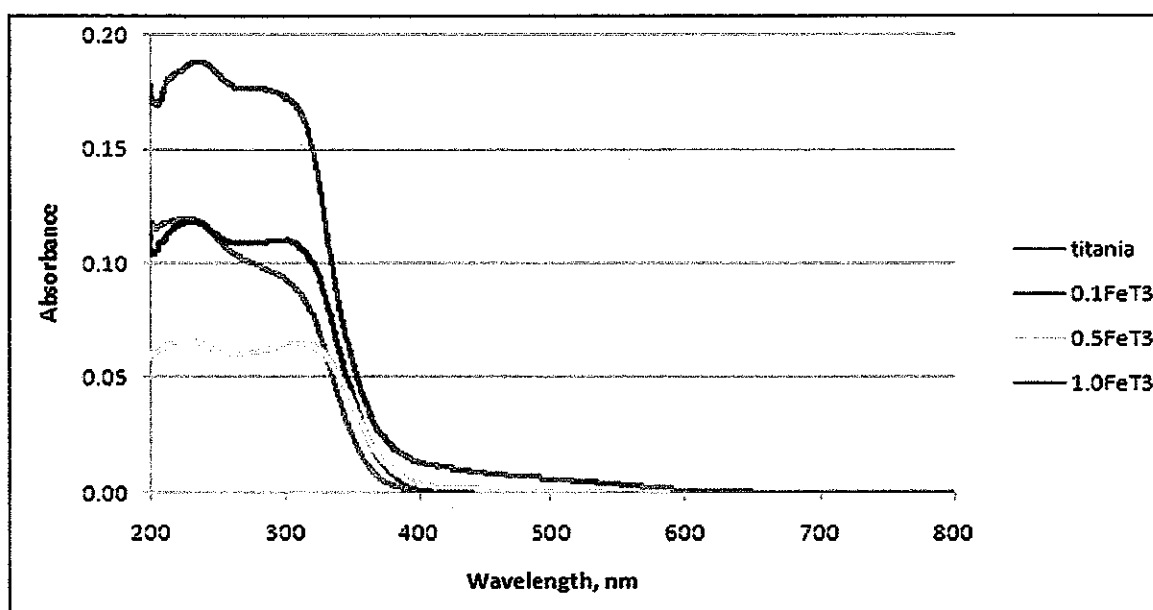
Figure 4.6: The DR-UV-Vis spectra of TiO_2 and $Fe\text{-}TiO_2$ calcined at $300^{\circ}C$

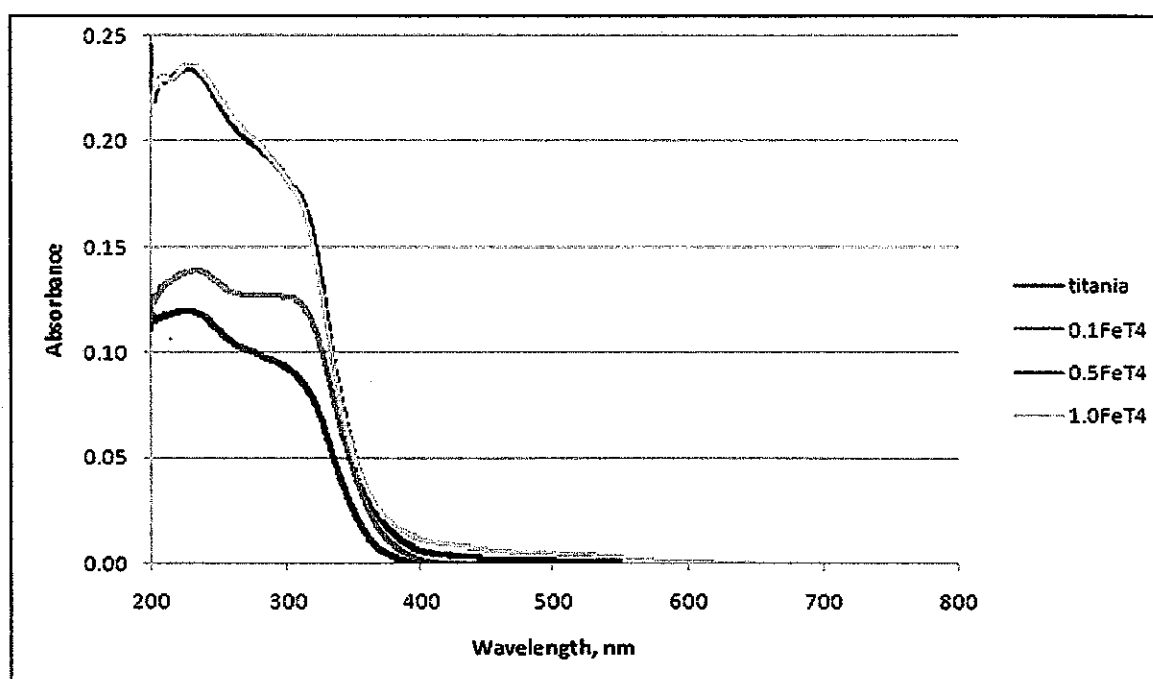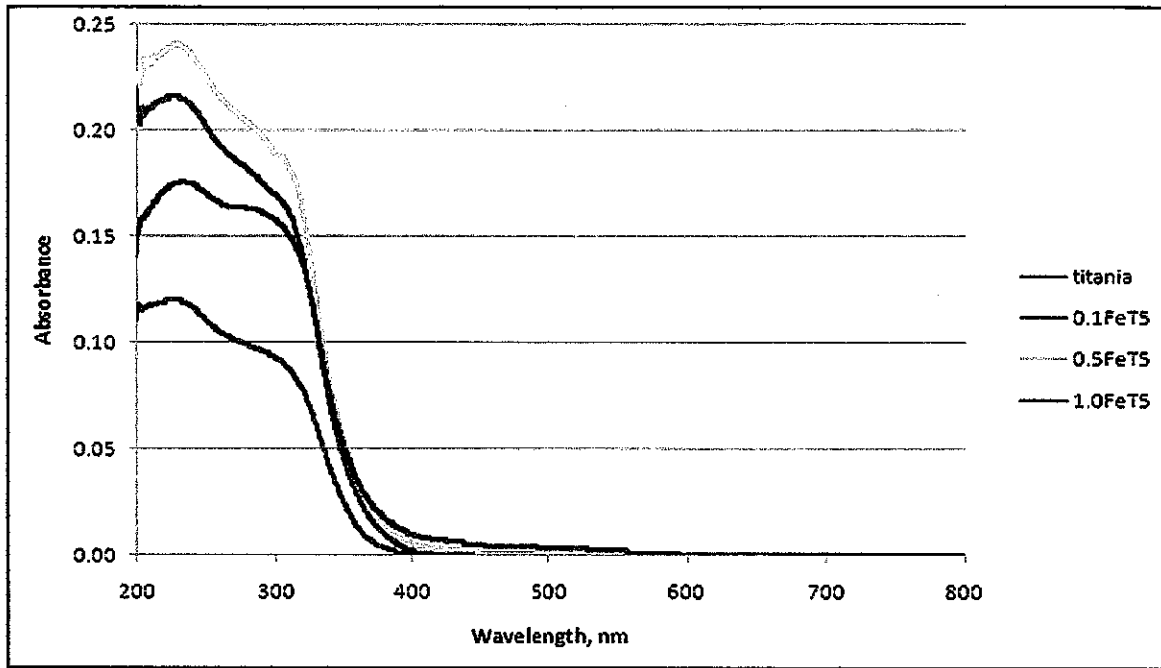Figure 4.7: The DR-UV-Vis spectra of TiO_2 and $Fe\text{-}TiO_2$ calcined at $400^{\circ}C$

Figure 4.8: The DR-UV-Vis spectra of TiO_2 and $Fe-TiO_2$ calcined at $500°C$

The diffuse reflectance spectra of all Fe-doped TiO_2 samples have extended a red shift and increased absorbance in the visible range with the increasing dopant content (Zhu *et al.*, 2004). Increased light absorption in the visible region possibly leads to better photocatalytic efficiency under visible light irradiation (Zhou *et al.*, 2006; Zhu *et al.*, 2004).

The absorption edges shift toward longer wavelengths indicates a decreased in the band gap energy for TiO_2 (Zhou *et al.*, 2006). The UV-Vis absorption edge and band gap energy of the samples have been determined by plotting the transformed Kubelka-Munk function $[F(R).hv]^{1/2}$ versus hv. The plot has shown a linear region just above the optical absorption edge. The relationship can be described as

$$[F(R).hv]^{1/2} = K\,(hv - E_g) \qquad \text{(Eq. 7)}$$

where hv = proton energy, E_g = the band gap energy, and K = a constant characteristic of the semiconductor material.

The extrapolation lines have been used to determine the band gaps for different loading of catalyst samples tested. The plot shown in the Figure 4.9 below is for the samples that are calcined at 300°C. Sample of calculation for band gap estimation from DR-UV-Vis spectra results is provided in Appendix C. From the extrapolation of the plot, the calculated band gap energy for pure TiO_2 is found to be 3.2 eV. The calculated values of the band gap energy are given in Table 4.1.
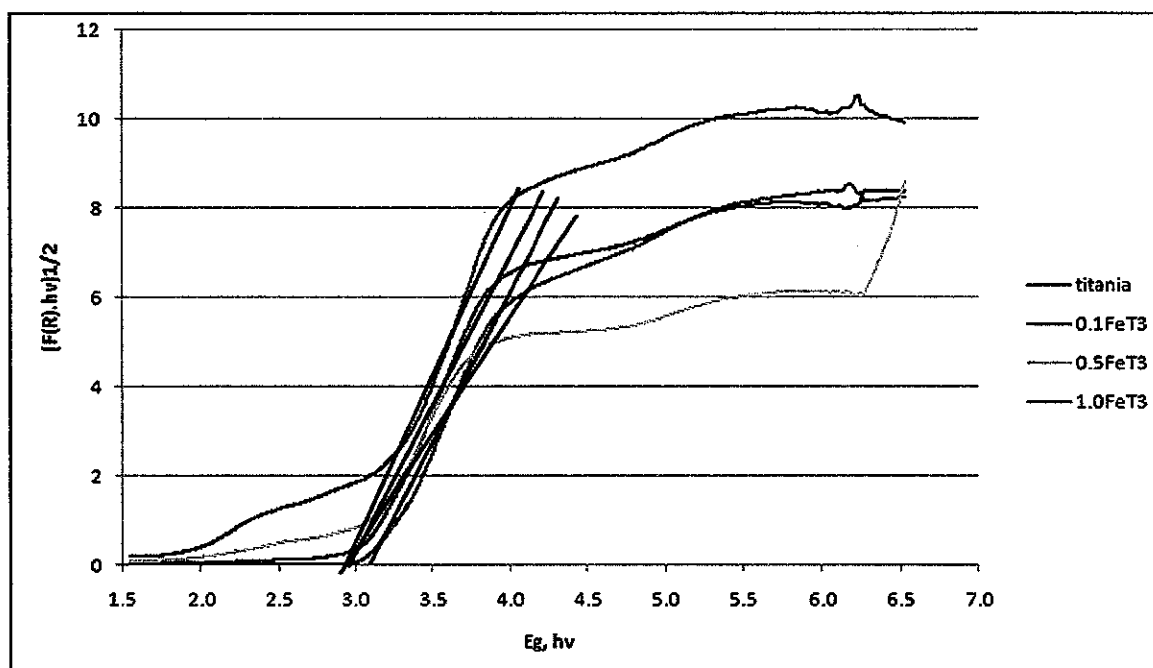

Figure 4.9 : Plot of transformed Kubelka-Munk functions $[F(R).hv]^{1/2}$ versus E_g for Fe-TiO_2 calcined at 300°C and pure TiO_2 to estimate band gap energy.

Table 4.1: Band gap energy for each catalyst prepared

Photocatalyst	Band gap energy (hv)
Titania (Degussa P25)	3.20
0.1FeT3	3.08
0.5FeT3	**2.98**
1.0FeT3	3.11
0.1FeT4	3.10
0.5FeT4	3.08
1.0FeT4	3.16
0.1FeT5	3.13
0.5FeT5	3.09
1.0FeT5	3.11

Based on the table, it clearly showed that all photocatalyst displayed reduction in their band gaps compare to pure TiO_2. The largest reduction is observed for 0.5FeT3 (2.98 eV). The photocatalyst also produced higher hydrogen generation compare to other photocatalyst prepared. Based on the table, it was clear that all 0.5 wt% photocatalyst have lower band gap compared to 0.1 wt% and 1.0 wt%.

4.2.4 Field Emission Scanning Electron Microscopy (FESEM)

Figure 4.2 (a)-(d) showed micrographs of photocatalyst 0.1 wt% and 0.5 wt% calcined at different temperature. The particle structures were found to be spherical, smooth and uniform. From the result, it is believed that the Fe clusters were evenly dispersed onto the support, TiO_2. The addition of glycerol during the preparation contributed to the high dispersion of Fe (Li *et al.*, 2006). Glycerol prohibits the aggregation of the Fe particle and favors the formation of highly dispersed metal oxide onto the support (Li *et al.*, 2006).
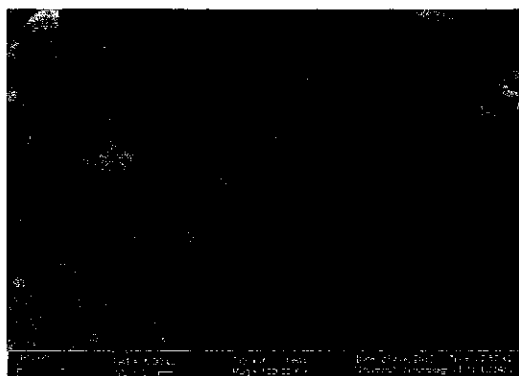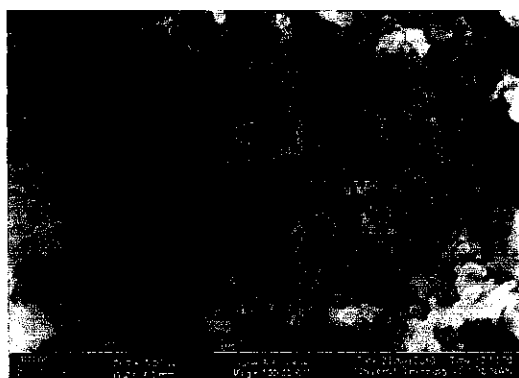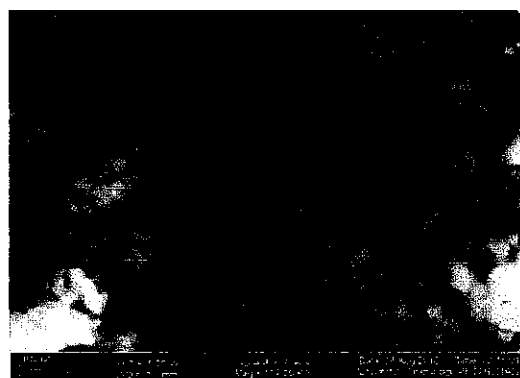
(a) 0.1FeT3
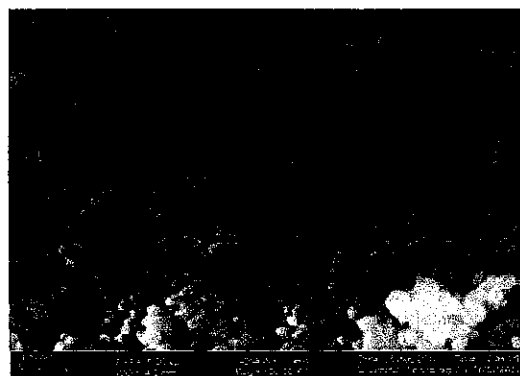
(c) 0.5FeT4

(b) 0.5FeT3

(d) 0.5FeT5

Figure 4.10: The FESEM micrographs of the Fe/TiO$_2$

4.2.5 X-ray Diffractometer (XRD)

Figure 4.11 showed the XRD patterns for Fe/TiO$_2$ photocatalyst. Two main peaks were observed in all samples at $2\theta = 25.4°$ and $27.5°$. The peaks respectively correspond to the main peak of anatase and rutile. Another crystal structure of TiO$_2$, brookite was not observed in the patterns. Pure TiO$_2$ Degussa P25 consisting of a mixture of anatase and

rutile in proportion of 70%/30% (Kirchernova *et al.*, 2005). It can be seen that with Fe-doping concentration increasing, the peak intensity of anatase slightly decreased.

Based on the peaks, we can see that Fe peak is not observed in all samples. One possible reason is that the concentration of Fe-doping is so low that it cannot be detected by XRD (Zhou *et al.*, 2006). However, since for 1.0 wt% Fe-loading, Fe peak is also not observed. The reason responsible to this is all the iron ions maybe insert into the structure of titanium, allowing uniform distribution of the Fe to form an iron-titanium oxide solid solution (Zhou *et al.*, 2006; Zhu *et al.*, 2004). This shows that Fe is well-dispersed on the photocatalyst.
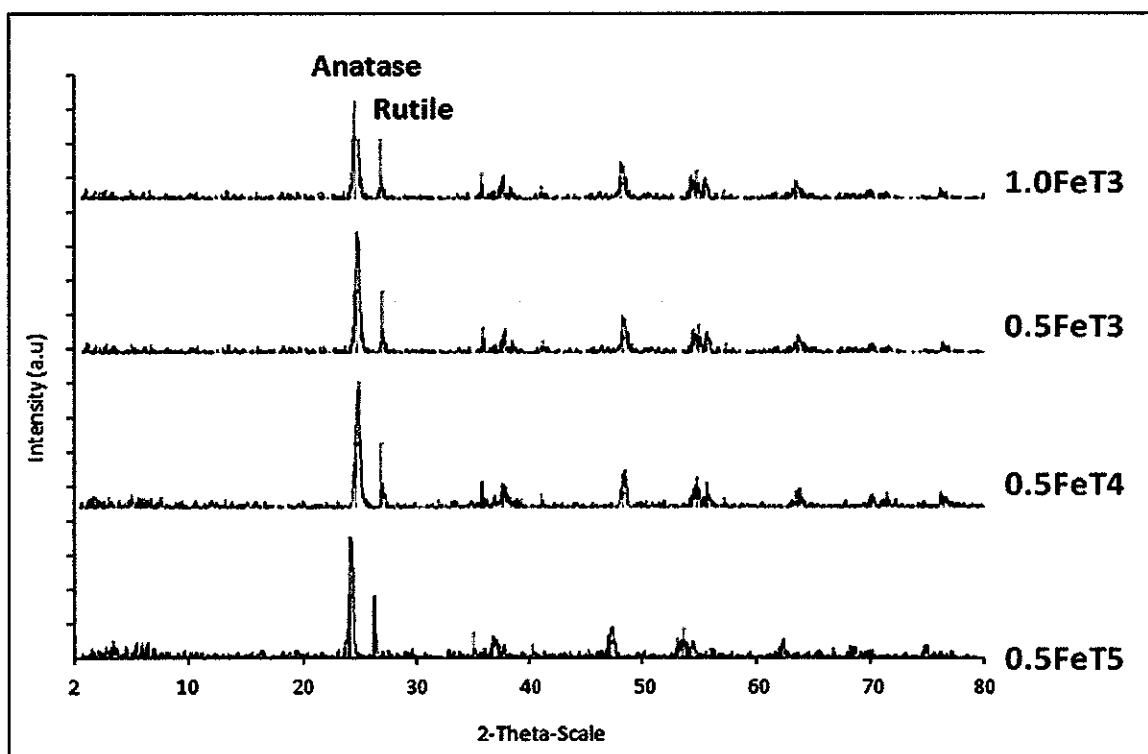

Figure 4.11: XRD diffractograms for Fe/TiO$_2$ photocatalyst after calcination

CHAPTER 5

CONCLUSION AND RECOMMENDATIONS

5.1 CONCLUSION

Fe/TiO_2 can absorb longer wavelength making it active under visible light compared to TiO_2. Doping with iron has shifted the absorption edge of TiO_2 towards the visible region (400 nm – 800 nm). Fe/TiO_2 displayed lower the band gap, resulting in increased of hydrogen production from water. 0.5 wt% of Fe/TiO_2 photocatalyst calcined at 300°C showed the highest H_2 production which is 5.75 mL in 2 hours compared to 2.5 mL using TiO_2. It also has the lowest band gap energy (2.98 eV) compared to the other photocatalyst prepared.

5.2 RECOMMENDATIONS

For further study, recommendations are based on three main things which are:

1) Preparation method
   - aging time to precipitate the raw catalyst
     For this project, aging time is 30 minutes. For future study, aging time should be longer to give time for raw catalyst to precipitate more.

   - different precipitating agent
     Sodium hydroxide has been using as precipitating agent in this project. Different precipitating agent such as sodium carbonate and ammonium hydroxide can be used to study the effect of different precipitating agent.

2) Type of metal ion doping
   - Different type of metal ion loading can be used to study the effect of metal doping to photocatalytic activity of photocatalyst.
3) Calcination time
   - For this project, calcination time used is one hour. To study the effect of calcination time to the photocatalyst, calcination time should be manipulated to obtain the optimum calcination time.

REFERENCES

Ambrus Zoltán, Balázs Nándor, Alapi Tünde, Wittmann Gyula, Sipos Pál, Dombi András, and Mogyorósi Károly, (2008). Synthesis, structure and photocatalytic properties of Fe(III)-doped TiO_2 prepared from $TiCl_3$, Applied Catalysis B, Environmental 81, pp 27-37.

Anonymous, (2009). Splitting Water into Hydrogen and Oxygen, http://www.alternative-energy-news.info/splitting-water-into-hydrogen-and-oxygen, 24th April 2010.

Anonymous, (2009). Understanding How Water Molecules Split, http://www.alternative-energy-news.info/understanding-how-water-molecules-split, 15th April 2010.

Dholam R., Patel N., Adami M. and Miotello A. (2009). Hydrogen production by photocatalytic water-splitting using Cr- or Fe-doped TiO_2 composite thin films photocatalyst, International Journal of Hydrogen Production Energy, 34, pp 5337-5346.

Drennen Thomas E. and Rosthal Jennifer E. (2007). *Pathways to a Hydrogen Future*, Elsevier, UK

Fernandes R., Patel N., Adami M. and Miotello A. (2009). Low energy ion-beam modification of TiO_2 photocatalyst thin film for visible light absorption, Surface & Coatings Technology, 203, pp 2579 – 2583.

Fujishima Akira, Rao Tata N. and Tryk Donald A. (2000). Titanium dioxide photocatalysis, Journal of Photochemistry and Photobiology C: Photochemistry Reviews, 1, pp 1-21.

Grimes Craig A., Oomman K. Varghese, and Sudhir Ranjan, (2008). *Light, Water, Hydrogen: The Solar Generation of Hydrogen by Water Photoelectrolysis*, Springer, New York.

Gupta Ram B. (2008). *Hydrogen Fuel: Production, Transport, and Storage*, CRC Press, USA.

Haag Werner O., Gates Bruce C. and Knozinger Helmut, (1999). *Advances in Catalysis*, Volume 44, Academic Press, UK.

Jiang Hongbo and Gao Lian, (2002). Enhancing the UV inducing hydrophilicity of TiO_2 thin film by doping Fe ions, Materials Chemistry and Physics, 77, pp 878 – 881.

Kirchnerova, J., Herrera Cohen, M.L., Guy, C. and Klvana D., (2005). Photocatalytic Oxidation of *n*-butanol under fluorescent visible light lamp over commercial TiO_2 (Hombicat UV100 and Degussa P25), Applied Catalysis A, General 282, pp 321-332.

Kudo Akihiko, (2006). Development of Photocatalyst Materials for Water Splitting, International Journal of Hydrogen Energy, 31, pp 197-202.

Li Y., Mei C., Jerry R., Yide X. and Wenjie S., (2006). Glycerol-mediated Synthesis of Ni an Ni/NiO Core-shell Nanoparticle, Materials Letter, 60, pp 750-753.

Lingsebigler Amy L., Guangquan Lu and John T. Yates, (1994). Photocatalysis on TiO_2 Surfaces: Principles, Mechanisms, and Selected Results, Chem. Rev ,95, pp 735-758.

Liu A.R., Wang S.M., Zhao Y.R. and Zheng Z. (2006). Low-Temperature Preparation of Nanocrystalline TiO_2 Photocatalyst with a Very Large Specific Surface Area, Materials Chemistry and Physics, 99, pp 131-134.

Mansor Anis, (2008). *Photocatalytic Degradation of Phenol in Aqueous Solution using Fe/TiO₂ Thin Films under UV and Visible Light*, Master Thesis, Universiti Sains Malaysia, Pulau Pinang, Malaysia.

Oh Seung-Min, Kim Seung-Se, Lee Ji Eun, Ishigaki Takamasa and Park Dong-Wha, (2003). Effect of additives on photocatalytic activity of titanium dioxide powders synthesized by thermal plasma, Thin Solid Films, 435, pp 252 – 258.

Photocatalytic Materials Inc, (unknown). How to Procedure Photocatalyst?', http://www.photocatalyst.co.jp/e/tukuru/tukuru.htm, 23rd March 2010.

Rajeshwar K., McConnell R. and Licht S. (2008). *Solar Hydrogen Generation: Toward a Renewable Energy Future,* Springer, USA.

Rand D. A. J. and Dell R. M. (2008). *Hydrogen Energy: Challenges and Prospects*, RSC Publishing, UK.

Regalbuto John, (2007). *Catalyst Preparation : Science and Engineering,* CRC Press, USA.

Sasikala R., Sudarsan V., Sudakar C., Naik R., Panicker L. and Bharadwaj S.R., (2009). Modification of the photocatalytic properties of self doped TiO₂ nanoparticles for hydrogen generation using sunlight type radiation, International Journal of Hydrogen Energy, 34, pp 6105 – 6113.

Sperling Daniel and Cannon James S. (2004). *The Hydrogen Energy Transition: Moving Toward the Post Petroleum Age in Transportation,* Elsevier, USA.

Viswanathan B., Sivasanker S. and Ramaswamy A.V. (2002). *Catalyst : Principles and Applications,* Narosa, New Delhi.

39

Yoong L.S., Chong F.K. and Binay K. Dutta, (2009). Development Of Copper-Doped TiO_2 Photocatalyst For Hydrogen Production Under Visible Light, Energy, 34, pp 1652-1661.

Zhou Mingua, Yu Jiagou and Cheng Bei, (2006). Effects of Fe-doping on the photocatalytic activity of mesoporous TiO_2 powders prepared by an ultrasonic method, Journal of Hazardous Materials, B137, pp 1838-1847.

Zhu Jiefang, Zheng Wei, He Bin, Zhang Jinlong and Anpo Masakazi, (2004). Characterization Of Fe–TiO_2 Photocatalysts Synthesized By Hydrothermal Method And Their Photocatalytic Reactivity For Photodegradation Of XRG Dye Diluted In Water, Journal of Molecular Catalysis A, Chemical 216, pp 35-43.

Zou Zhigang, Ye Jinhua, Sayama Kazuhiro and Arakawa Hironori, (2001). Direct Splitting of Water under Visible Light Irradiation with an Oxide Semiconductor Photocatalyst, http://www.nature.com/nature/journal/v414/n6864/abs/414625a.html?lang=en, 15th April 2010.

APPENDIX A

Catalyst Preparation

Table 3.2 : Molecular Weight for chemicals involves in catalyst preparation

Chemicals	Molecular Formula	Molecular Weight (g/mol)
Iron (III) Nitrate	$Fe(NO_3)_3.9H_2O$	404.00
Iron Metal	Fe	55.85
Titanium Dioxide	TiO_2	79.87
Glycerol	$C_3H_5(OH)_3$	92.094

Table 3.3 : Summary of mass for respective loading

Content	Fe (III) loading (wt%)		
	0.1	0.5	1.0
Amount of catalyst (g)	20	20	20
Mass of Fe (g)	0.02	0.1	0.2
Mass of TiO_2 (g)	19.98	19.9	19.8
Mass of $Fe(NO_3)_3.9H_2O$ (g)	0.1447	0.7234	1.4467
Volume of glycerol (ml)	0.0523	0.2617	0.5235

Sample of calculation for 0.1wt% Fe-TiO$_2$

Basis: 20g of catalyst

For   100g catalyst $\rightarrow$ 0.1g of Fe metal

      20g of catalyst $\rightarrow$ x

So,

$$x = \frac{20\text{g of catalyst}}{100\text{g of catalyst}} \times 0.1\text{g of Fe metal}$$

$$= 0.02 \text{ g of Fe metal}$$

Hence, 1 mol of Fe(NO$_3$)$_3$.9H$_2$O $\rightarrow$ 55.85g of Fe

Y mol of Fe(NO$_3$)$_3$.9H$_2$O $\rightarrow$ 0.02g of Fe

$$Y = \frac{0.02\text{g of Fe}}{55.85\text{g of Fe}} \times 1 \text{ mol of Fe(NO}_3)_3. 9\text{H2O}$$

$$= 0.000358102 \text{ mol of Fe(NO}_3)_3.9\text{H}_2\text{O}$$

The amount of Fe(NO$_3$)$_3$.9H$_2$O is:

1 mol of Fe(NO$_3$)$_3$.9H$_2$O $\rightarrow$ 404g/mol

0.000358102 mol of Fe(NO$_3$)$_3$.9H$_2$O $\rightarrow$ Z

$$Z = \frac{0.000358102 \text{ mol of Fe(NO}_3)_3. 9\text{H2O}}{1 \text{ mol of Fe(NO}_3)_3. 9\text{H2O}} \times 404\text{g/mol}$$

$$= 0.1447\text{g of Fe(NO}_3)_3.9\text{H}_2\text{O}$$

42

Sample calculation of glycerol (0.1wt% Fe-TiO₂)

Note that;

Glycerol: $Fe(NO_3)_3.9H_2O = 2:1$

2 mol of glycerol = 1 mol of $Fe(NO_3)_3.9H_2O$

A mol of glycerol = 0.000358102 mol of $Fe(NO_3)_3.9H_2O$
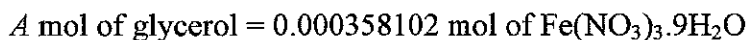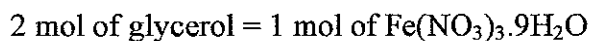
$$A = \frac{0.000358102 \text{ mol of } Fe(NO_3)_3.9H2O}{1 \text{ mol of } Fe(NO_3)_3.9H2O} \times 2 \text{ mol of glycerol}$$

= 0.000716204 mol of glycerol

The amount of glycerol is:

1 mol of glycerol → 92.094g of glycerol

0.000716204 mol of glycerol → B
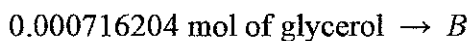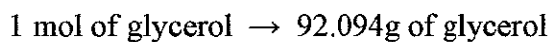
$$B = \frac{0.000716204 \text{ mol of glycerol}}{1 \text{ mol of glycerol}} \times 92.094 \text{g of glycerol}$$

= 0.0660g of glycerol

Convert to ml

Density of glycerol = 1.26 g/ml

$$\text{Volume of glycerol (ml)} = \frac{\text{Mass of glycerol (g)}}{\text{Density of glycerol } (\frac{g}{ml})}$$

$$= \frac{1g}{1.26g/ml}$$

$$= 0.79365 \text{ ml}$$

So,

1 g of glycerol $\rightarrow$ 0.79365 ml of glycerol

0.0660g of glycerol $\rightarrow$ C ml of glycerol

$$C = \frac{0.0660g \text{ of glycerol}}{1 \text{ g of glycerol}} \times 0.79365 \text{ ml of glycerol}$$

$$= 0.0523 \text{ ml of glycerol}$$

APPENDIX B

Calculation and Preparation of 0.25M NaOH

a) NaOH Mass Calculation

M.W for NaOH = 40 g/mol

$$\text{Numbers of mol (mol)} = \frac{\text{mass (g)}}{\text{M.W} \left(\frac{g}{mol}\right)}$$

$$\text{Molarity} = \frac{\text{Numbers of mol (mol)}}{\text{Volume (L)}}$$

Substitute first equation into second equation:

$$\text{Molarity} = \frac{\text{Mass (g)} \times \text{M.W} \left(\frac{g}{mol}\right)}{\text{Volume (L)}}$$

So, $\quad \text{Mass (g)} = \text{Molarity (M)} \times \frac{\text{M.W} \left(\frac{g}{mol}\right)}{\text{Volume (L)}}$

$$\text{Mass (g)} = 0.25\ \text{M} \times \frac{40 \frac{g}{mol}}{1\ \text{L}}$$

$$= 10\ \text{g of NaOH}$$

b) Preparation of 1L NaOH Stock Solution

1) 10 g of NaOH palettes were measured using the electronic weighing scale.
2) Then, the palettes were transferred into 500 ml beaker and diluted with distilled water.
3) The diluted solution was poured into 1000 ml volumetric flask, and distilled water was added slowly until the solution reaches the marker.

APPENDIX C

Band Gap Estimation from DR-UV-Vis Spectra Results

a) DR-UV-Vis spectra for TiO_2
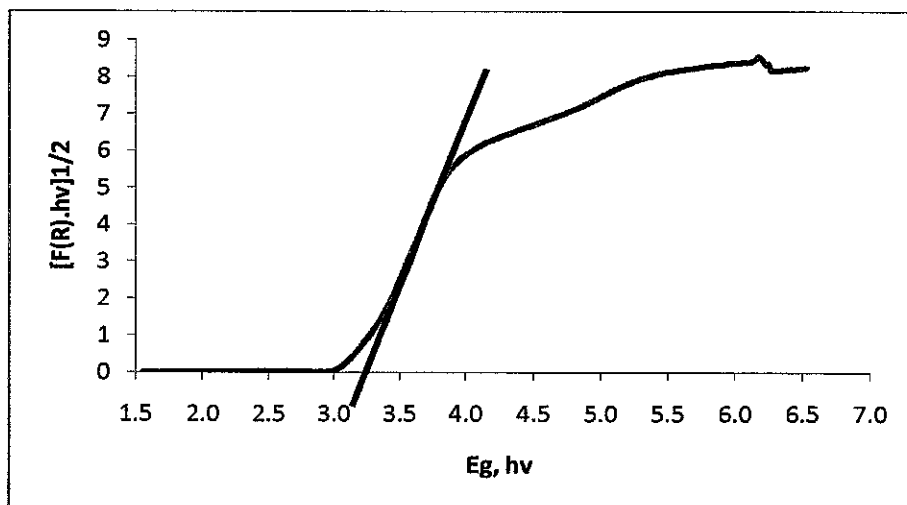
The band gap for TiO_2 is determined using the extrapolation of the absorption edge onto the energy axis (E_g) using the linear equation, $y = mx + c$.

From the extrapolation linear curve, two plots were obtained which were (3.50733, 2.60821) and (3.67361, 4.02122).

$$m = \frac{4.02122 - 2.60821}{3.67361 - 3.50733} = 8.49777$$

Insert (3.50733, 2.60821) into $y = mx + c$

$2.60821 = 8.49777 (3.50733) + c$

$c = -27.19629$

So, $y = 8.49777x - 27.19629$

When $y = 0$, $x = 3.20$

Therefore, the estimated band gap for TiO_2 is 3.20 eV.